Journal of Power Sources 257 (2014) 394–401

Contents lists available at ScienceDirect

Journal of Power Sources

journal homepage: www.elsevier.com/locate/jpowsour

Sensitivity analysis of a mathematical model of lithium–sulfur cells part I: Applied discharge current and cathode conductivity

Mahmoudreza Ghaznavi, P. Chen*

Department of Chemical Engineering and Waterloo Institute for Nanotechnology, University of Waterloo, 200 University Avenue West, Waterloo, Ontario N2L3G1, Canada

HIGHLIGHTS

- The discharge behavior of Li–S cells in a wide range of current rate is studied.
- Sulfur must highly dissolve in electrolyte to maintain high capacity performance.
- A threshold of cathode's conductivity exists bellow which the cell would not operate.
- Above the conductivity threshold no capacity loss is observed due to conductivity.

ARTICLE INFO

Article history:
Received 8 July 2013
Accepted 9 October 2013
Available online 8 November 2013

Keywords:
Lithium–sulfur battery
Modeling battery
Simulations
Cathode conductivity

ABSTRACT

A sensitivity analysis of a mathematical model of a lithium-sulfur (Li–S) battery was performed, focusing on the effects of the discharge current and the electronic conductivity of the cathode by investigating the response of the model to variations of these parameters over a wide range of values. The behavior of the model battery system with respect to the variations of each parameter is explained in detail. The nonlinear response of the model to the parameter variations is presented. In particular, the discharge current causes different patterns of the voltage plateaus. The importance of the electronic conductivity of the cathode is also discussed in detail. A minimum conductivity requirement to activate the cell was observed, beyond which no significant improvement of the capacity performance occurs. This report evaluates the electrochemical aspects of different experimental results particularly regarding discharge voltage plateaus, and moreover, demonstrates the limits of the model.

1. Introduction

The lithium–sulfur (Li–S) battery is a promising energy storage system because sulfur, the active material, has a high theoretical specific energy (2600 Wh kg^{-1}); furthermore, sulfur is inexpensive, abundant, and nontoxic. Over the past decade, extensive efforts have focused on developing a rechargeable Li–S battery [1]. However, no Li–S battery has been commercialized to date due to several unsolved problems. Because of the insulating nature of the Li–S battery discharge products, namely, sulfur and lithium sulfides (Li_2S_2, Li_2S), a relatively high amount of conductive material must be added to the Li–S battery cathode to guarantee the utilization of the active material [2]. In addition, the dissolved polysulfides in the electrolyte diffuse through the separator to the lithium anode and react directly with the lithium. This reaction creates the so-called internal shuttle phenomenon, which causes passivation of active material and the self-discharge of the battery [1–3].

Although a wide range of experimental strategies have attempted to tackle these problems, little theoretical attention has been paid to understanding the mechanism of the Li–S battery. Moreover, the behavior of the sulfur as the active material is very complicated and extremely sensitive to the different physical and chemical parameters involved in the preparation of the cathode composite or even during the assembly of a cell [2,4–6]. For example, very complex reduction reactions of elemental sulfur, S_8, occur during the discharge processes, and different polysulfide chains form in as-yet-undetermined ways [4–6]. Although the exact reduction reaction mechanism is not yet definitively determined, some models have been introduced to describe Li–S batteries. Y. V. Mikhaylik et al. [7] developed a mathematical model for the shuttle effect based on a two-stage reduction of sulfur. Specifically, S_8 reduces to S_4^{2-}, and S_4^{2-} reduces to S_2^{2-} and S^{2-}. The direct

* Corresponding author. Tel.: +1 519 888 4567x35586; fax: +1 519 888 4347.
E-mail addresses: mghaznavi@uwaterloo.ca (M. Ghaznavi), p4chen@uwaterloo.ca (P. Chen).

0378-7753/$ – see front matter © 2013 Elsevier B.V. All rights reserved.
http://dx.doi.org/10.1016/j.jpowsour.2013.10.135

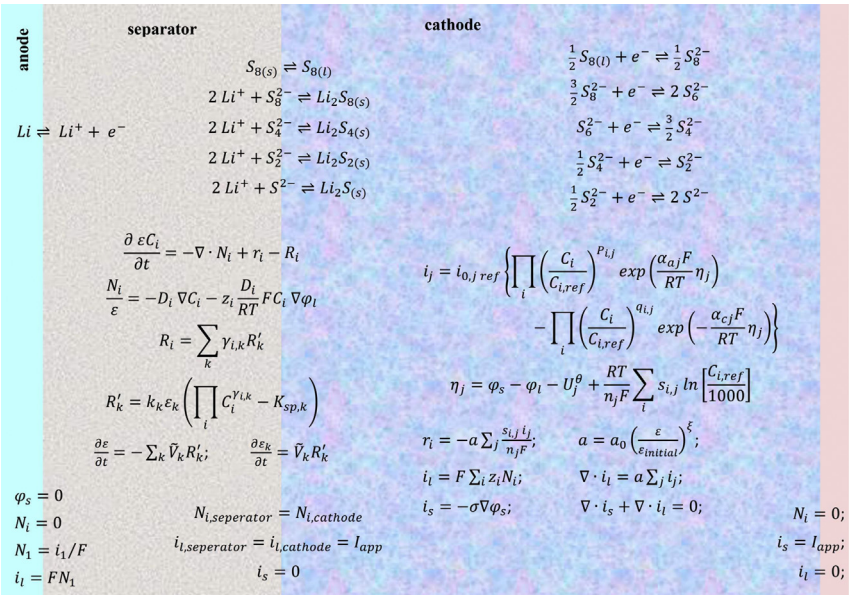

Fig. 1. Schematic of a Li–S cell and a summary of the governing equations and boundary conditions.

reduction of high-polysulfides on the surface of the lithium anode was also included in the model. The model produced a good understanding of the shuttle effect, thus providing evidence that the self-discharge, overcharge, and efficiency are strongly related to the shuttle effect.

Another mathematical model, introduced by K. Kumaresan et al. [8], considered five different stages for the reduction of sulfur to mathematically describe the discharge behavior of Li–S batteries. The model considers the dissolution and precipitation of sulfur and polysulfides into the electrolyte. Assuming that the electrochemical reactions in the system follow the Butler–Volmer equation, the equations governing the material balance of each individual species are solved in the model. The authors assumed many different parameters that must be determined by proper experiments, but in the absence of such experimental results, they provided educated guesses for most of the parameters. Nevertheless, their results corresponded well with a class of experimental results.

In fact, the behavior of sulfur batteries strongly depends on the morphology [9] and chemical properties of the cathode composite and electrolyte chosen [2]. Therefore, changing the additives in the cathode composite [2,9,10] or electrolyte [2,11] leads to different discharge plateau shapes. Two flat discharge plateaus are observed in most cathode composites of sulfur and carbon materials [2]. In contrast, in the cathode composites made of sulfur and polymer materials, only one decreasing plateau typically appears in the discharge duo in the interaction between sulfur and polymer [10,12]. Even within the two categories, significant changes occur in the details of the discharge plateau in different experiments. Despite the difficulty of doing so, investigating a specific system using the model of Kumaresan et al. requires that each parameter be determined through an analysis of the results of experiments on that system. Conversely, because of the system's complexity, different sets of parameters may result in the same model output. A sensitivity analysis of the model parameters will help elucidate the model and identify the actual Li–S cell behavior. The results of a sensitivity analysis would identify a range of values for each physical parameter and, more importantly, a set of possible physical or chemical properties responsible for a specific behavior of the cell.

The aim of this paper is not only to investigate the possible ranges of the physical parameters by performing a sensitivity analysis but also to explore the mathematical validation of the model and thus clarify its abilities and limits. The results of the sensitivity analysis can be used to improve the mathematical model and can ultimately contribute to the development of commercial Li–S batteries.

This article is the first part of a series on the sensitivity analysis of the model presented by Kumaresan et al. In this article, the focus is on the response of the model to variations in the discharge current. Furthermore, the electronic conductivity of the cathode, one of the major issues in Li–S batteries, is studied in detail. The dynamics of the active material in the solid phase is investigated to estimate the cyclability of the Li–S cell.

2. Model development and governing equations

The model is based on the proposed model by K. Kumaresan, Y. Mikhaylik, and R. E. White [8]. Fig. 1 presents a schematic of the Li–S cell and summarizes the governing equations and boundary conditions of the model. Appendix B describes the model, and Appendix A defines its parameters. The values proposed for the parameters are provided in Tables 1–4 in Appendix C.

The reactions in the cell include Li metal oxidization at the anode surface during discharge [8]:

$$\mathrm{Li} \rightleftharpoons \mathrm{Li}^+ + e^- \tag{1}$$

It is assumed that during discharge, the elemental sulfur, which is initially in the solid phase, dissolves in the electrolyte and then goes through the following electrochemical reactions [8]:

$$\frac{1}{2}\mathrm{S}_{8(l)} + e^- \rightleftharpoons \frac{1}{2}\mathrm{S}_8^{2-} \tag{2}$$

$$\frac{3}{2}\mathrm{S}_8^{2-} + e^- \rightleftharpoons 2\mathrm{S}_6^{2-} \tag{3}$$

$$\mathrm{S}_6^{2-} + e^- \rightleftharpoons \frac{3}{2}\mathrm{S}_4^{2-} \tag{4}$$

$$\frac{1}{2}\mathrm{S}_4^{2-} + e^- \rightleftharpoons \mathrm{S}_2^{2-} \tag{5}$$

$$\frac{1}{2}S_2^{2-} + e^- \rightleftharpoons 2S^{2-} \quad (6)$$

The following precipitation/dissolution reactions are also present:

$$S_{8(s)} \rightleftharpoons S_{8(l)} \quad (7)$$

$$2Li^+ + S_8^{2-} \rightleftharpoons Li_2S_{8(s)} \quad (8)$$

$$2Li^+ + S_4^{2-} \rightleftharpoons Li_2S_{4(s)} \quad (9)$$

$$2Li^+ + S_2^{2-} \rightleftharpoons Li_2S_{2(s)} \quad (10)$$

$$2Li^+ + S^{2-} \rightleftharpoons Li_2S_{(s)} \quad (11)$$

The details of the model and its governing equations can be found either in Appendix B or Ref. [8]. The current densities due to the electrochemical reactions are given by the Butler–Volmer equation.

3. Results and discussion

A range of variations is assumed for each parameter. This range is not bounded by a range of physical values. The goal is to determine the behavior of the model system with respect to different situations and also to find a range for the parameters in which the Li–S cells are feasible. However, the functionality of the model with respect to these parameters was found not to be linear. Instead, we must choose a parameter each time and investigate the changes in the model from variations in this parameter while keeping the other parameters constant.

3.1. Applied discharge current, I_{app}

One of the important goals in battery research is to widen the discharge current operation range of batteries; for example, a particularly high current rate is required for electric vehicles. Moreover, the discharge voltage plateau of a battery and its cyclability are strongly dependent on the current rate during operation. Therefore, the response of the model to a range of applied currents must be investigated.

Fig. 2 presents the discharge voltage plateaus. In the first three discharge currents, with low applied discharge currents, I_{app} = 0.02C, 0.05C, and 0.1C, two voltage plateaus are very clear, and the voltage curves are quite similar, except from a decreasing shift in potential. This similarity indicates that the kinetics of the chemical reactions is almost the same at these rates of discharge. Because the decrease in the potential due to the resistivity of the cathode matrix and electrolyte is very small ($<10^{-4}$ V) compared to the total decrease in potential, one may conclude that the kinetics of the chemical reactions causes the decrease. In other words, the decrease is due to polarization at the surface of the anode and cathode. The linear approximation of the Butler–Volmer equation (Equation (B5)) describes a linear relationship between the decrease in potential and change in current ($\Delta i \propto \Delta V$) and thus well approximates the observed plateaus in the first three discharge currents.

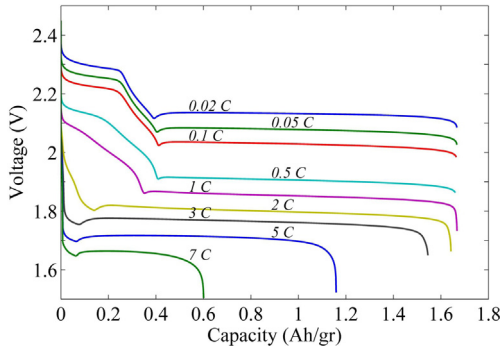

Fig. 2. The discharge plateau of a sulfur-based cell at different discharge current rates. First plateau vanishes due to low dissolution rate of elemental sulfur.

The first plateau starts to deform at the discharge rate of 0.05C, as the speed of dissolution of elemental sulfur into the electrolyte is too slow to maintain a constant concentration of dissolved sulfur. The slow dissolving rate of sulfur is the main reason for the capacity loss, which starts at 2C. Fig. 3 provides more details of the reactions kinetics of the Li–S system. The normalized current, which is due to electrochemical reaction j in the cathode and is defined by the following expression, is used to illustrate the system's kinetics:

$$I_j^N = \frac{1}{I_{app}} \int_{x=L_s}^{x=L} a i_j \mathrm{d}x \quad (12)$$

where $\sum_{j=2}^{6} I_j^N = 1$. In other words, I_j^N represents the overall contribution of the electrochemical reaction j in producing the discharge current at a given time. In the ideal case of utilizing the entire capacity of sulfur, the discharge normalized currents satisfy the following relations:

$$\frac{1}{T_{DC}} \int_{t=0}^{T_{DC}} I_j^N \mathrm{d}t = C_j, \quad (13a)$$

$$\{C_2, \ldots, C_6\} = \left\{\frac{1}{8}, \frac{1}{24}, \frac{1}{12}, \frac{1}{4}, \frac{1}{2}\right\} \quad (13b)$$

where T_{DC} is the total time of an ideal complete discharge and C_j is the portion of reaction j in the total capacity. The average concentration of the sulfide species at the cathode is presented in Fig. 4. Because the graphs of normalized current for the cases I_{app} = 0.1C and 0.05C are similar to the case of 0.02C, they are not shown in Fig. 3, whereas the concentration of the sulfide species in these cases are shown (dotted lines) to illustrate the difference in the second part of the discharge. As the discharge current rate increases to 0.1C, the concentration of the high sulfides ($S_{8(l)}$, S_8^{2+}, and S_6^{2+}) decreases more in the second part than in the first part because more material is used in the reaction. Thus, a higher concentration of the low sulfides (S_4^{2+}, S_2^{2+}, and S^{2+}) forms before the rate of the low-sulfide reactions becomes sufficiently high and the precipitation of Li_2S begins. This sequence of events causes a small shift in the sharp trough between the two stages. The shift in precipitation toward the right occurs even for a discharge current rate of 0.5C, for which the trough starts to shift because the low-sulfide reaction begins relatively sooner. The relatively fast resolution of sulfur to electrolyte maintains a constant sulfur concentration during the first stage, and therefore, a constant reaction rate was observed. The reduction of S_8^{2-} occurs simultaneously with a constant rate because the reference voltage is similar. When the solid sulfur in the system is fully consumed, the concentration of sulfur decreases suddenly (in the related time scale), as does the related current. At this point, the second reaction reaches a sharp peak in its time scale and quickly reduces almost all of the S_8^{2-}. The reduction of S_6^{2-} becomes the dominant reaction in the system, leading to the

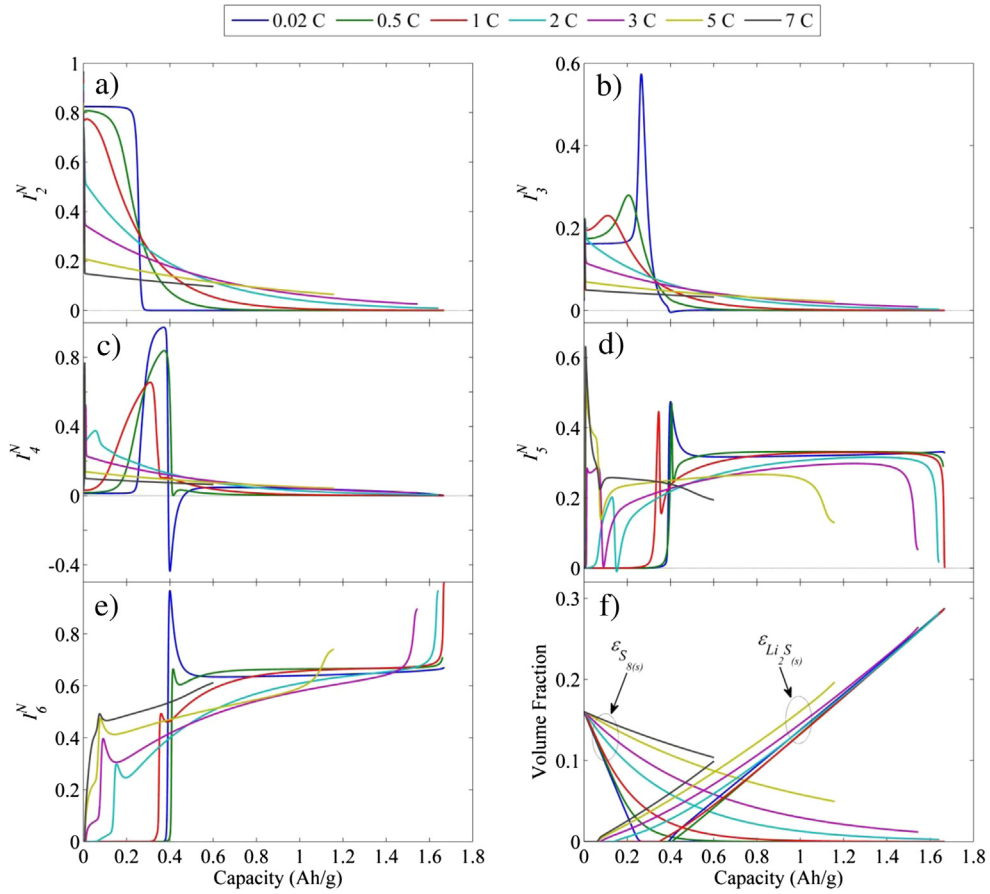

Fig. 3. (a), (b), (c), (d), and (e) Normalized current (see Equation (12)), due to different electrochemical reactions, produced by the reduction of $S_{8(l)}$, S_8^{2-}, S_6^{2-}, S_4^{2-}, and S_2^{2-}, respectively. (f) Average volume fraction of solid elemental sulfur, $\varepsilon_{S_{8(s)}}$, and $Li_2S_{(s)}$, $\varepsilon_{Li_2S_{(s)}}$, in the cathode during discharge. Unutilized elemental sulfur is the main reason of capacity lost in high C rates.

production of the lower sulfides. As a result, the concentration of the low sulfides increases; therefore, the reaction requires a higher polarization at the cathode's surface. The potential of the cell consequently decreases to a local minimum in a sharp trough. At the point at which Li_2S starts to precipitate, the concentration of S^{2-} decreases, causing a sharp increase in rate of the last two reactions. Interestingly, because the S_4^{2-} concentration is high for the related potential, a reverse reaction occurs for the high sulfides. Upon reaching a quasi-steady state, the rate of the last two reactions becomes constant during the remaining discharge time. However, the third reaction continues slowly. Once all of the sulfides have been reduced, a sudden drop in the potential occurs.

For a discharge current of 0.5C and higher, sulfur dissolution is too slow to maintain a constant concentration of elemental sulfur in the electrolyte solution. Thus, the other reactions begin correspondingly sooner in their time scales, creating smoother peaks and drops. However, up to a 1C discharge rate, the dissolution is sufficiently fast to keep the first (and second) reaction dominant during the first stage of discharge, but those reactions continue in the second part of the discharge because some solid sulfur is still present that can be dissolved into the electrolyte solution. The reverse reactions then cease due to the earlier start of the low-sulfide reactions in their relative time scales. Although the sharp troughs in potential and in the concentrations of high sulfides and concentration peaks of the low sulfides still exist when S^{2-} precipitation starts (for the reasons explained earlier), the sharp trough in the high-sulfide concentrations is no longer due to a reverse reaction. Instead, this trough now occurs as the species consumption rate drops due to a reduction reaction, concurrent with the production due to the dissolving of sulfur. The dependence of the dissolution/precipitation of each species on the nucleus size of each precipitate is clearly observed in the volume fraction of elemental sulfur, which does not exhibit a linear decrease.

Starting from 2C, elemental sulfur does not dissolve sufficiently fast to maintain even the first two reactions as the system's dominant reactions. The low-sulfide reductions start earlier, and the low-sulfide concentrations reach their maximum levels very quickly. Again, the start of the S^{2-} precipitation causes the sharp trough in the levels of the high-sulfide concentrations and the peaks in low-sulfide concentrations. Whereas the high-sulfide reaction rates change smoothly over time, the reduction of S_4^{2-} exhibits a sharp trough at this starting point of precipitation and the last reaction reaches a peak. The dissolution of elemental sulfur does not occur sufficiently quickly: the solid sulfur particles dissolve more slowly as they become smaller. Thus, the sulfide species cannot be produced in the quantities required to be involved in the reactions, causing the potential to drop and the end of discharge, and some unused solid sulfur remains in the cathode.

At low discharge rates, the species concentration is nearly uniform in the cell because diffusion proceeds faster than the production and consumption. However, at high C rates, gradients in the concentration of the species are generated across the cell to produce the essential mass transfer. For all the species, except S^{2-} and $S_{8(l)}$, the maximum concentration is at the interface of the anode

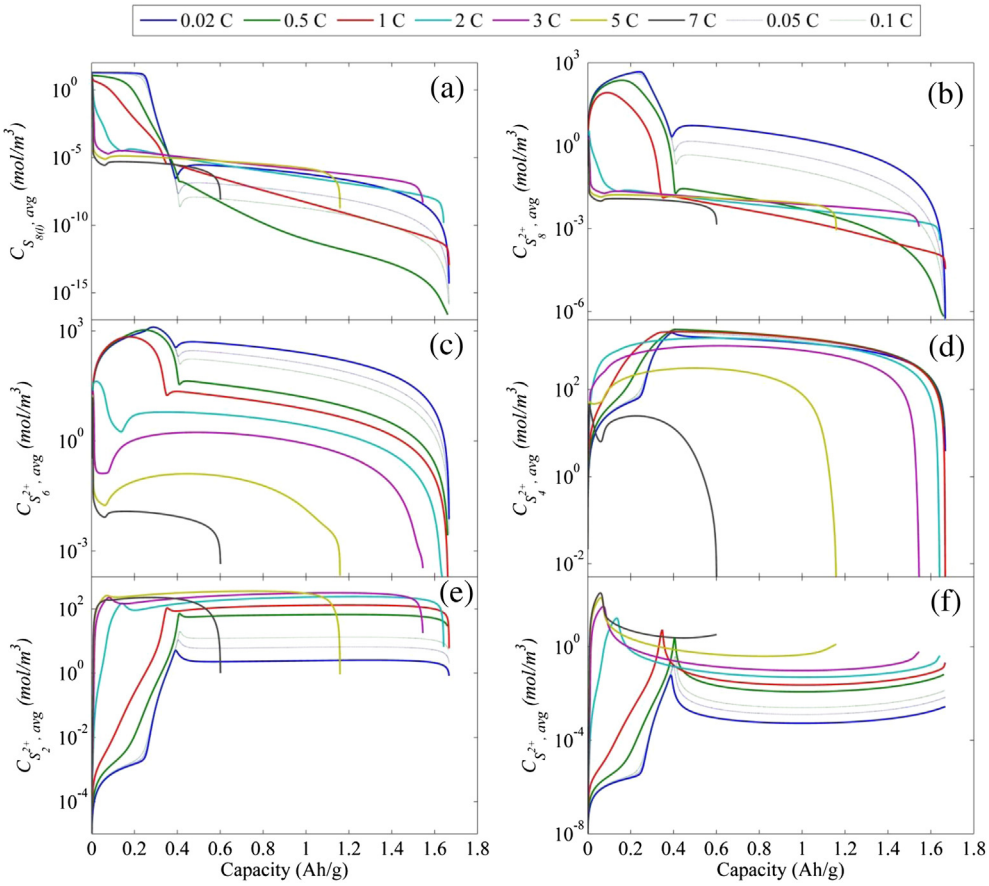

Fig. 4. Average concentration of the relevant species in the cathode during discharge. Increasing the discharge rate, the concentrations of high polysulfides decrease and the concentrations of low polysulfides increase.

and separator. The concentration gradients have higher slopes at the separator than at the cathode. The S^{2-} concentration exhibits the same behavior before precipitation starts but drops at both the separator and cathode once precipitation starts. However, comparing the concentrations in both areas, the S^{2-} concentration remains higher at the cathode because of its simultaneous production. Consequently, a concentration gradient forms at the cathode-separator interface. In contrast, a high concentration of S^{2-} and Li^{+} at the anode and separator interface causes a relatively high precipitation of $Li_2S_{(s)}$ at the anode surface soon after discharge begins. Fig. 5 shows the volume fraction of $Li_2S_{(s)}$ across the cell at different discharge times, at $I_{app} = 7C$. At $t = 10$ s, the volume fraction is almost zero everywhere. At $t = 20$ s, the volume fraction begins to increase and has a large maximum at the anode surface. Over time, the precipitation continues everywhere in the cathode because the production of S^{2-} occurs at that location. Moreover, the diffusion of S^{2-} into the separator causes $Li_2S_{(s)}$ to form deep in the separator (for the same reason, the volume fraction in the cathode at a short distance from the interface is less than that deep inside the cathode). However, the higher concentration of Li^{+} at the interface causes a $Li_2S_{(s)}$ volume fraction peak to form at a short distance from the interface inside the cathode. This information elucidates the stresses in the cell and the deformation of the cathode during cycling.

3.2. Conductivity of the cathode, σ

Neither sulfur nor polysulfides are conductive; therefore, the cathode must consist of a conductive porous matrix that holds sulfur in its pores and facilities the accessibility of electrons to the sulfur. The method of manufacturing the conductive matrix is one of the major difficulties in sulfur-based cell fabrication: on the one hand, a higher conductivity requires more conductive additives and less sulfur in the cathode, causing the cell to lose its specific energy capacity; on the other hand, lower conductivity causes reduced utilization of the sulfur as the active material. This section investigates the effect of the conductivity of the porous matrix on the cell performance. No difference in the matrix porosity is assumed; only the conductivity was varied. This investigation approach matches the situations in which the conductive additive is changed but not the amount used, assuming the porosity remains the same.

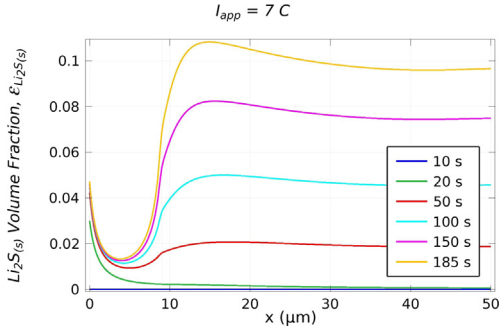

Fig. 5. Volume fraction of $Li_2S_{(s)}$, $\varepsilon_{Li_2S_{(s)}}$ across the cell at different times of discharge with a current rate of 7C. The interface of the separator and the cathode is located at $x = 9$ μm.

Fig. 6 illustrates the effect of the conductivity of the cathode porous media matrix on the battery performance. The upper and lower sets of lines represent the voltage plateaus for a 1C and 5C discharge rate, respectively. The conductivity of the cathode matrix is assumed to vary from 1 S m^{-1} to 10^{-4} S m^{-1}. For the discharge rate of 5C, the simulation result for $\sigma = 10^{-4}$ S m^{-1} did not converge to a solution at times longer than approximately 2 s, i.e., it is not possible to discharge at a high C rate when the conductivity is not sufficiently high. The graphs indicate that once a certain conductivity threshold has been exceeded, no significant change occurs to the voltage plateau if the conductivity is increased further, indicating the dominant role of the reaction kinetics in the cell behavior. As the conductivity decreases, an unexpected drop in potential at the beginning of the cell discharge was observed. This drop is more obvious at a rate of 1C. At low conductivity, the potential gradient in the cathode matrix is steep (unlike at high conductivity), with a minimum at the interface of the cathode and current collector. Therefore, a steep gradient in the concentration of the species is required for a well-distributed electrochemical reaction across the cathode. As the cell discharge begins because the species concentration is uniform, a sharp drop in the potential of the solid matrix forms at the interface of the cathode and current collector to draw all of the current from this region. Over time, the production of more ions in the electrolyte causes a gradient in the concentration of species to form, leading to more-distributed electrochemical reactions across the cathode. However, the peak of the reactions still exists at that interface, but it is not as sharp as before. At the end of the discharge, the smaller number of ions again causes to a sharp potential drop to form at the interface. The high rate of low-sulfide production at the interface leads to a high-rate of precipitation as well such that precipitated species fill the porous regions. Fig. 7 presents the volume fraction of $Li_2S_{(s)}$ at the separator and cathode during discharge. The porous medium, at the interface of the cathode and current collector, is clearly completely filled by the precipitant. One may conclude that this filling phenomenon causes the active material to be lost in the cycling because the solid sulfur at that area does not have easy access to the electrolytes.

4. Conclusions

A sensitivity analysis of a mathematical model of a Li–S cell with respect to the discharge current rate and the conductivity of the cathode matrix was performed, the results of which provided details on the different characteristics of the cell. Depending on the discharge current (and the availability of dissolved sulfur), the relevant electrochemical reactions can occur either simultaneously

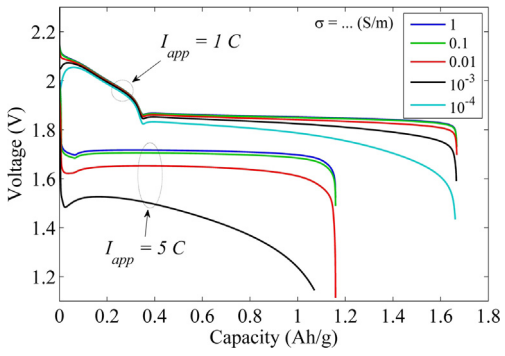

Fig. 6. The discharge plateaus of the sulfur-based cell with different conductivities of the cathode matrix for discharge current rates of 5C and 1C.

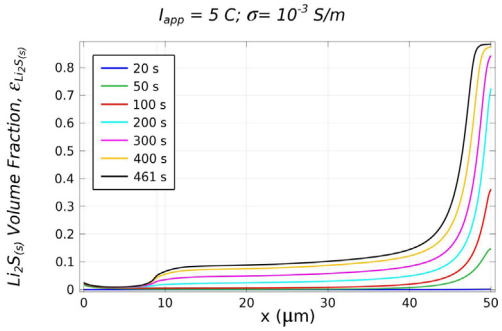

Fig. 7. Volume fraction of $Li_2S_{(s)}$, $\varepsilon_{Li_2S_{(s)}}$ across the cell at different times of discharge for a discharge current rate of 5C. The separator-cathode interface is located at $x = 9$ μm.

or after the previous reactions have completed. The coincidence or non-coincidence of the electrochemical reactions determines the shape of the discharge plateau. Sharp changes in the voltage plateau are observed when the electrochemical reactions occur non-coincidentally, whereas a smooth plateau is expected in the coincidental case. In particular, if the first plateau has vanished, one may verify the existence of the first plateau by decreasing the discharge current. If the plateau appears at a low discharge rate, slow dissolution of elemental sulfur into the electrolyte causes a significant capacity loss. The details of the effects of precipitation rate constant on the cell behavior will be studied in part III of this series of papers. The simulation results also demonstrate a partial movement of the active material into the separator during discharge.

To functionalize the cell, a minimum in the cathode conductivity is required (depending on the discharge current) below which the cell would not operate and above which no capacity loss is observed due to the conductivity. Low conductivity only causes a steeper discharge voltage, particularly at the beginning and end of discharge.

The model predicts a very flat second plateau, which differs from the results of many experiments. This difference is a direct consequence of assuming that all the surfaces in the cathode are active surfaces for electrochemical reactions, ignoring the non-conductive nature of the solid sulfur and polysulfides. The model needs to be improved by including active surface loss due to the precipitation of polysulfides.

Acknowledgments

Financial support for this work was provided by Positec, the Natural Sciences and Engineering Research Council of Canada (NSERC), Canada Foundation for Innovation (CFI), and the Canada Research Chairs (CRC) program. The authors are grateful to The Nam Long Doan for very useful discussions.

Appendices

A. Parameters and symbols (primarily taken from Ref. [5])

a	specific surface area of the cathode
a_0	initial value of a
b	Bruggeman coefficient
c_i	concentration of species i ($i = Li^+, S_{8(l)}, S_8^{2-}, S_6^{2-}, S_4^{2-}, S_2^{2-}, S^{2-}$, and A^- (anion of the lithium salt used in the electrolyte)), mol m^{-3}
$c_{i,\mathrm{ref}}$	reference concentration of species i, mol m^{-3}

C_j portion of reaction j in the total capacity for an ideal complete discharge
$D_{i,0}$ diffusion coefficient of species i in the bulk medium, $m^2\ s^{-1}$
D diffusion coefficient of species i in the porous medium, $m^2\ s^{-1}$
F Faraday constant, C $equi^{-1}$
i_j current density due to reaction j, A m^{-2}
$i_{j,ref}$ exchange current density of the electrochemical reaction j at the reference concentrations, A m^{-2}
i_l superficial current density in the liquid phase, A m^{-2}
i_s superficial current density in the solid phase, A m^{-2}
I_{app} applied current density, A m^{-2}
I_j^N normalized current due to electrochemical reaction j
$K_{sp,k}$ solubility product of precipitate k
k_k rate constant of precipitate k
L thickness of the cell, m
L_s thickness of the separator, m
N_i superficial flux of species i, mol $m^2\ s^{-1}$
n_j number of electrons transferred in electrochemical reaction j
$p_{i,j}$ anodic reaction order of species i in electrochemical reaction j
$q_{i,j}$ anodic reaction order of species i in electrochemical reaction j
R gas constant, J $mol^{-1}\ K^{-1}$
R_i production rate of species i due to precipitation reactions, mol $m^3\ s^{-1}$
R'_k rate of precipitation of solid species k, mol $m^3\ s^{-1}$
r_i production rate of species i due to electrochemical reactions, mol $m^3\ s^{-1}$
$s_{i,j}$ stoichiometric coefficient of species i in electrochemical reaction j
T temperature, K
T_{DC} total time of an ideal complete discharge, s
t time, s
U_j^θ standard open circuit potential (OCP) of electrochemical reaction j
$U_{j,ref}$ OCP of electrochemical reaction j at reference concentrations, V
$\tilde{V}_k$ Molar volume of the precipitate k, $m^3\ mol^{-1}$
z_i charge number of species i
α_{aj} anodic transfer coefficient of reaction j
α_{cj} cathodic transfer coefficient of reaction j
ε porosity of the separator and cathode
ε_k volume fraction of precipitate k in the separator and cathode
φ_l potential in the liquid phase, V
φ_s potential in the solid phase, V
$\gamma_{i,k}$ number of ionic species i produced by dissociation of precipitate k
η_j overpotential for electrochemical reaction j
σ effective conductivity of the solid phase of the cathode, S m^{-1}
ξ morphology parameter

B. Governing equations

The model includes the electrochemical reactions given by Equations (1)–(6) and the precipitation/dissolution reactions given by Equations (7)–(11). In a porous medium, the governing equation for the material balance of an individual species is

$$\frac{\partial \varepsilon C_i}{\partial t} = -\nabla\cdot N_i + r_i - R_i \tag{B1}$$

where the flux is given by

$$\frac{N_i}{\varepsilon} = -D_i\nabla C_i - z_i\frac{D_i}{RT}FC_i\nabla\varphi_l \tag{B2}$$

The diffusion coefficient for species i, D_i, is corrected based on Bruggeman's expression for porosity and tortuosity: $D_i = D_{i,0}\varepsilon^b$. The rate of production/consumption of species i due to the electrochemical reactions can be written in the form

$$r_i = a\sum_j \frac{s_{ij}i_j}{n_jF} \tag{B3}$$

where the stoichiometric coefficients are given in Table 1, Appendix C. The specific surface area of the cathode varies due to the precipitation/dissolution of the various lithium sulfide species and is assumed to be governed by the empirical expression:

$$a = a_0\left(\frac{\varepsilon}{\varepsilon_{initial}}\right)^{\xi} \tag{B4}$$

where the empirical parameter, ξ, is assigned a value of 1.5. The Butler–Volmer equation yields the current density due to the electrochemical reactions:

$$i_j = i_{0,j\ ref}\left\{\prod_i\left(\frac{C_i}{C_{i,ref}}\right)^{P_{i,j}}\exp\left(\frac{\alpha_{aj}F}{RT}\eta_j\right) - \prod_i\left(\frac{C_i}{C_{i,ref}}\right)^{q_{i,j}}\exp\left(-\frac{\alpha_{cj}F}{RT}\eta_j\right)\right\} \tag{B5}$$

where the overpotential for the reaction j is

$$\eta_j = \varphi_s - \varphi_l - U_{j,ref} \tag{B6}$$

The terms $p_{i,j} = s_{ij}$ refer to anodic species and $q_{i,j} = -s_{ij}$ refer to cathodic species. The open-circuit potential for reaction j is given by

$$U_{j,ref} = U_j^\theta - \frac{RT}{n_jF}\sum_i s_{i,j}\ln\left[\frac{C_{i,ref}}{1000}\right] \tag{B7}$$

The liquid phase current density is given by

$$i_l = F\sum_i z_iN_i \tag{B8}$$

The solid phase current density follows Ohm's law

$$i_s = -\sigma\nabla\varphi_s \tag{B9}$$

Because the charge can enter or leave the liquid phase only by electrochemical reactions, the following equations apply at the liquid/solid interface:

$$\nabla\cdot i_l = a\sum_j i_j \tag{B10}$$

and

$$\nabla\cdot i_s + \nabla\cdot i_l = 0 \tag{B11}$$

The rate of consumption or production of species i due to precipitation/dissolution is related to the rate of precipitation/dissolution reaction k by

$$R_i = \sum_k \gamma_{i,k} R'_k \tag{B12}$$

where the rate of precipitation of solid species k is assumed to be governed by the following kinetic equation:

$$R'_k = k_k \varepsilon_k \left(\prod_i C_i^{\gamma_{i,k}} - K_{\mathrm{sp},k} \right) \tag{B13}$$

The volume fraction of the precipitate, k, is a function of time and is given by

$$\frac{\partial \varepsilon_k}{\partial t} = \tilde{V}_k R'_k \tag{B14}$$

Therefore, the porosity variation with time is

$$\frac{\partial \varepsilon}{\partial t} = -\sum_k \tilde{V}_k R'_k \tag{B15}$$

The boundary conditions of the model are as follows. At the interface of the cathode and the current collector, $x = L$, the BCs are

$$N_i = 0 \tag{B16a}$$

$$i_\mathrm{s} = I_\mathrm{app} \tag{B16b}$$

$$i_\mathrm{l} = 0 \tag{B16c}$$

At the cathode-separator interface, $x = L_s$,

$$N_{i,\mathrm{seperator}} = N_{i,\mathrm{cathode}} \tag{B17a}$$

$$i_{\mathrm{l,\ seperator}} = i_{\mathrm{l,\ cathode}} = I_\mathrm{app} \tag{B17b}$$

$$i_\mathrm{s} = 0 \tag{B17c}$$

At the surface of anode, $x = 0$,

$$\varphi_\mathrm{s} = 0 \tag{B18a}$$

$$N_i = 0 \tag{B18b}$$

$$N_1 = i_1/F \tag{B18c}$$

$$i_l = FN_1 \tag{B18d}$$

The governing equations can be solved numerically.

C. Parameter tables for reference values

Table 1
Stoichiometric coefficients, S_{ij} [8].

S_{ij}	Reactions given by equation (j)					
Species (i)	1	2	3	4	5	6
Li^+	−1	0	0	0	0	0
$S_{8(l)}$	0	−1/2	0	0	0	0
S_8^{2-}	0	1/2	−3/2	0	0	0
S_6^{2-}	0	0	2	−1	0	0
S_4^{2-}	0	0	0	3/2	−1/2	0
S_2^{2-}	0	0	0	0	1	−1/2
S^{2-}	0	0	0	0	0	1
A^-	0	0	0	0	0	0

Table 2
Kinetic and thermodynamic properties [8].

Reaction (j)	$i^*_{0,j\ \mathrm{ref}}$ (A m^{-2})	α^*_{aj}	α^*_{cj}	n_j	U_j^θ
1	0.394	0.5	0.5	1	0.0
2	1.9719	0.5	0.5	1	2.39
3	0.019719	0.5	0.5	1	2.37
4	0.019719	0.5	0.5	1	2.24
5	1.972×10^{-4}	0.5	0.5	1	2.04
6	1.972×10^{-7}	0.5	0.5	1	2.01

Table 3
Transport properties and reference concentrations [8].

Species (i)	z_i	D^*_{i0} (m^2 s^{-1})	$C^*_{i,\ \mathrm{ref}}$ (mol m^{-3})
Li^+	+1	1×10^{-10}	1001.08
$S_{8(l)}$	0	10×10^{-10}	19.0
S_8^{2-}	−2	6×10^{-10}	0.1832
S_6^{2-}	−2	6×10^{-10}	0.3351
S_4^{2-}	−2	1×10^{-10}	0.02146
S_2^{2-}	−2	1×10^{-10}	5.999×10^{-7}
S^{2-}	−2	1×10^{-10}	9.94×10^{-10}
A^-	−1	4×10^{-10}	1000

Table 4
Separator and cathode parameters [8].

Parameter	Separator	Cathode
Thickness (m)	9×10^{-6}	41×10^{-6}
$\varepsilon_{\mathrm{initial}}$	0.37	0.778
$\varepsilon_{S_{8(s)},\mathrm{initial}}$	1×10^{-12}	0.160
$\varepsilon_{Li_2S_{8(s)},\mathrm{initial}}$	1×10^{-6}	1×10^{-6}
$\varepsilon_{Li_2S_{4(s)},\mathrm{initial}}$	1×10^{-6}	1×10^{-6}
$\varepsilon_{Li_2S_{2(s)},\mathrm{initial}}$	1×10^{-6}	1×10^{-6}
$\varepsilon_{Li_2S_{(s)},\mathrm{initial}}$	1×10^{-7}	1×10^{-7}
a_0	–	132,762

Table 5
Parameters for the precipitation reactions, either assumed or from Ref. [8].

Precipitate (k)	Rate constant (k^*_k)	Solubility product (K^*_k)	Molar volume ($\tilde{V}_k$(m^3 mol^{-1}))
$S_{8(s)}$	1.0 s^{-1}	19.0 mol m^{-3}	1.239×10^{-4}
$Li_2S_{8(s)}$	1×10^{-11} m^6 mol^2 S^{-1}	18,3400 mol^3 m^{-3}	1.361×10^{-4}
$Li_2S_{4(s)}$	9.98×10^{-12} m^6 mol^2 S^{-1}	21,480 mol^3 m^{-3}	7.415×10^{-5}
$Li_2S_{2(s)}$	9.98×10^{-9} m^6 mol^2 S^{-1}	0.6006 mol^3 m^{-3}	4.317×10^{-5}
$Li_2S_{(s)}$	6.875×10^{-5} m^6 mol^2 S^{-1}	9.95×10^{-4} mol^3 m^{-3}	2.768×10^{-5}

References

[1] B. Ellis, K.T. Lee, L.F. Nazar, Chem. Mater. 22 (2010) 691–714.
[2] Sheng S. Zhang, J. Power Sources 231 (2013) 153–162.
[3] Xiulei Ji, Linda Nazar, J. Mater. Chem. 20 (2010) 9821–9826.
[4] D.H. Han, et al., J. Electrochem. Soc. 151 (9) (2004) E283–E290.
[5] C. Barchasz, et al., Anal. Chem. 84 (2012) 3973–3980.
[6] V.S. Kolosnitsyn, E.V. Karaseva, Russ. J. Electrochem. 44 (5) (2008) 506.
[7] Y. Mikhaylik, J.R. Akridge, J. Electrochem. Soc. 151 (11) (2004) A1969.
[8] K. Kumaresan, Y. Mikhaylik, R.E. White, J. Electrochem. Soc. 155 (8) (2008) A576.
[9] B. Zhang, et al., Energy Environ. Sci. 3 (2010) 1531–1537.
[10] T.N.L. Doan, et al., J. Power Sources 241 (2013) 61–69.
[11] K. Jeddi, M. Ghaznavi, P. Chen, J. Mater. Chem. A 1 (2013) 2769–2772.
[12] J. Fanous, Chem. Mater. 23 (2011) 5024–5028.